SMAR 2019 – Fifth Conference on Smart Monitoring,
Assessment and Rehabilitation of Civil Structures

SMAR 2019

Piezoelectric Wafers' Placement Optimization on Tubular Structures – Towards Application on Pipelines

Zainab ISMAIL [1], Samir MUSTAPHA [1], Hussein TARHINI [1]
[1] The American University of Beirut, Beirut, Lebanon

Contact e-mail: sm154@aub.edu.lb (Dr. Samir Mustapha)

ABSTRACT: This paper presents an extension of a model, which we have developed for optimization of the number and locations of piezoelectric wafers network on convex and non convex structures, to tubular structures. The proposed objective function is to maximize the coverage of the network on the structure that is discretized to a set of control points, while minimizing the number of piezoelectric (PZT) wafers. The tubular structure is modelled as a plate of any given dimensions with the appropriate boundary conditions imposed.

In the optimum solution, each control point should be covered by a user-defined number of sensing paths, defined as the coverage level. During the optimization process, any location on the plate is considered as a potential position for a PZT wafer. The algorithm provides the flexibility of changing a wide range of parameters including the number of PZT wafers, the distance covered around the sensing path, the required coverage level and the number of control points. Moreover, since the structure is continuous, the wave can propagate in every direction. Thus, a pair of PZT elements can communicate in two directions and can cover the control points lying in the neighborhood of its two corresponding paths. The developed model was solved using genetic algorithm.

Sensor network configurations were simulated on pipe sections. The results were promising and they demonstrated the proficiency of the developed model in distributing the PZT wafers on curved structures.

1 INTRODUCTION

Oil and water transport pipelines require ongoing maintenance and inspection as they are susceptible to damage due to harsh environmental conditions and loading during operation. The 2014 age distribution of oil pipelines in Europe, published by CONCAWE, showed that a 4.7% of the total, was 10 years old and 61.0% was over 40 years old (Davis, Spence et al. 2016). CONCAWE classifies spill causes into five major categories including mechanical failure, operational, corrosion, natural hazard and third party. The main causes of incidents are very different for hot and cold pipelines, whereas 81% of hot oil pipeline spillages are related to corrosion.

Pipe quality inspection is a necessity to ensure adequate performance during service. Over the years many non-destructive testing (NDT) methods have been developed and commonly used to control the quality of structural components after manufacturing, also to check structural integrity during the life of service. Common NDT methods include visual inspection and tapping, thermography, radiography and shearography, eddy-current, electromagnetic and electromechanical, and ultrasonics.

Monitoring of large structures, such as pipelines buried underground and long span bridges, is associated with many challenges starting with the difficulty of deployments of a large number of sensors along the enormous effort to collect and manage large amount of data that may be received continuously. In the last three decades a lot of work has focused on ultrasonic guided waves for detection and assessment as they are sensitive to both surface and embedded structural damage. They have proven proficiency, having been widely used to develop various damage identification algorithms for assessing delamination, de-bonding, holes, cracks/notches and corrosion in both composite and metallic plate-like structures (Mustapha, Ye et al. 2011).

An attractive alternative to point or single location measurements, for actuation and sensing of ultrasonic waves, which require the physical movement of the transducer, is the placement of sensors on several defined positions and then excite stress waves which will propagate along the pipe in the form of cylindrical Lamb waves (Silk and Bainton 1979). The response of the signal is then monitored along the pipe to identify any changes in the received signal. Due to the circular wave propagation along the wall of the pipe and the wave interaction with the annular cross section, the guided waves are sensitive to the depth, axial and circumferential extent of the defects (Cawley 2007). A large amount of research focused on the development of models and optimization techniques for sensor network optimization for optimal distribution of actuating and sensing points. The placement of a sensor network over a structure would provide a richer data, and helps in localizing and assessing flaws within the monitored structure.

This study aims to extend the model which was previously developed, in our laboratory, for sensor network optimization on convex/non-convex structures (Ismail, Fakih et al. 2018, Tarhini, Itani et al. 2018), to tubular structures towards the application in SHM. The model takes into account the waves propagation characteristics such as the wave propagation distance and the path coverage, as well as the geometrical constraints. The circular tube was modelled as a flat plate with the necessary boundary conditions imposed. The model was validated using a pipe section, which will be validated experimentally.

2 GUIDED WAVES IN TUBULAR STRUCTURES

The analytical foundation of guided waves in a three dimensional hollow cylinder of infinite extent was established by Gazis in 1959 (Gazis 1959) where a general solution for the displacement field components of wave particles in long hollow cylinders was presented. Due to the curvature in pipes and the dispersion characteristics, wave propagation in this type of structure is complex, with an infinite number of possible wave modes. The multimode guided waves can propagate along different paths including circumferential/flexural F(m, n), longitudinal L(0,n) and through the thickness of the pipe or torsional T(0, n) (Demma, Cawley et al. 2004). Due to these properties, guided waves have presented potential capacity for detecting different types of damage on both the inner and the outer surfaces of the pipe (Guan, Lu et al. 2017).

Figure 1 shows the group velocity dispersion curves for schedule 20, 203.2 mm diameter ASTM A106 seamless pressure pipe with the wall thicknesses of 6.35 mm (which was used in this study), using a MATLAB code developed by Seco et al. (Seco and Jiménez 2012). Axisymmetric modes, including longitudinal and torsional modes, are attractive for non-destructive testing. In particular, L(0, 2) mode travels faster than the other modes and is nondispersive within a wide range of frequencies (Gazis 1959). L (0, 2) is superior in detecting changes in the depth and along the circumference (Wang, Peter et al. 2010). Also, it has a simple acoustic field and can be easily excited (Verma, Mishra et al. 2014). Although, L (0, 1) generally exists along with L (0, 2), it can be filtered out as it travels at a slower group velocity.

Based on the above, the L (0, 2) mode will be used in our study. The coverage and the propagation distance of this mode were concluded, based on an experimental analysis using an excitation frequency of 200 kHz, to be 30 mm (on each side of the sensing path) and one meter, respectively.

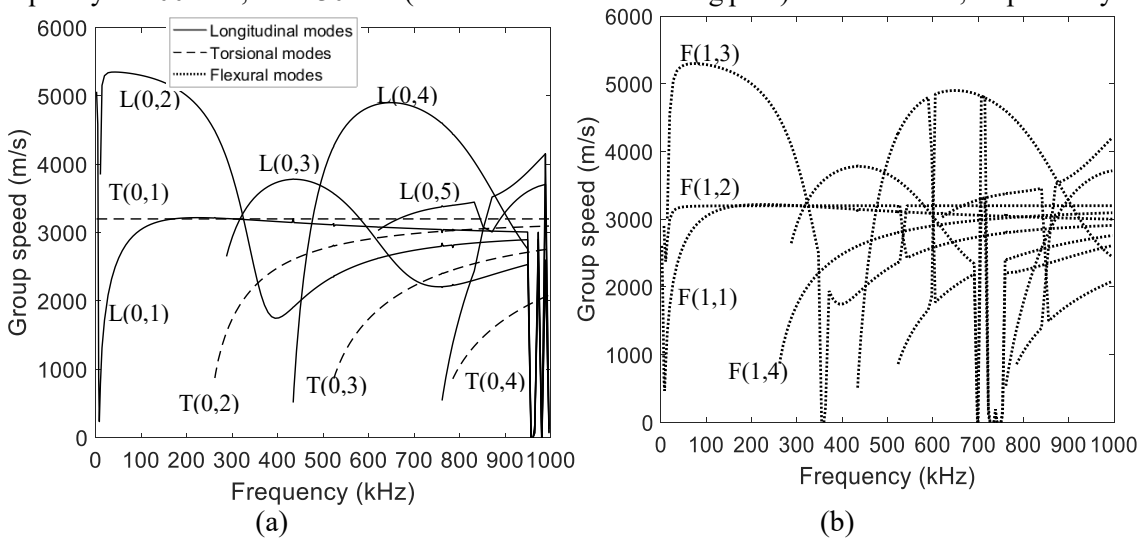

Figure 1. Group velocity dispersion curves in a pipe section: (a) longitudinal and torsional modes and (b) flexural modes.

3 METHODOLOGY

The optimization of the sensor network on the curved structure will be done by unfolding the surface on a 2-d plane. The proposed optimization algorithm aims to maximize the coverage of a predefined set of control points. The coverage level (n), which is a parameter chosen according to the user's requirements, is defined as the number of sensing paths required to cover a control point in order to be considered as covered. Huang and Tseng (Huang and Tseng 2005) stated that an accurate damage localization requires the coverage of three sensing paths ($n = 3$).

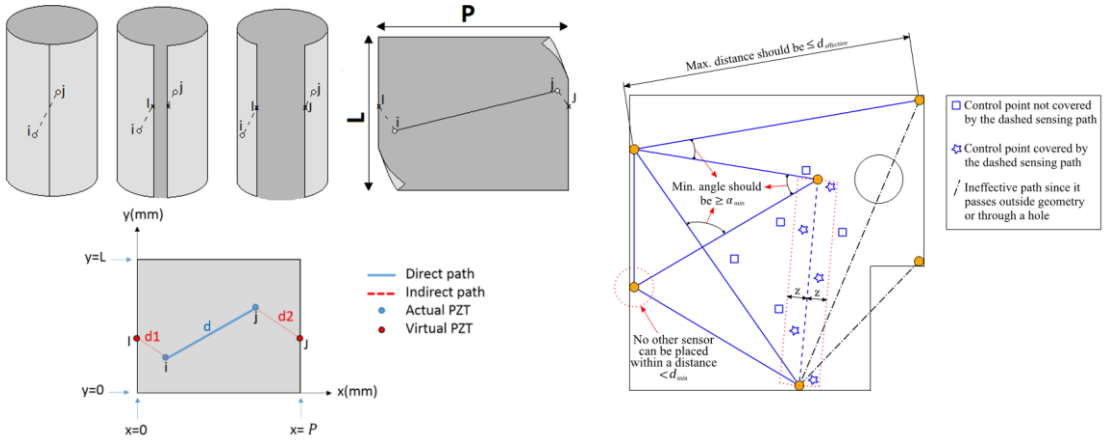

Figure 2. Illustration of the optimization model.

A sensing path (defined by any pair of PZTs) covers a control point if it lies within a given distance from the centerline of the path which is 0.03 m in our case. Other constraints include the structure's geometry, the number of available PZT wafers (N), the minimum distance between each two PZTs ($d_{min} = 0.03$ m) to avoid having multiple PZTs at the same location, and the

minimum angle between two sensing paths ($\alpha_{min} = 10°$) to ensure that the sensing paths are not collinear. Further, a maximum spacing between the actuator-sensor pair $d_{effective}$ was defined to account for the attenuation in the wave signal. Finally, a maximum propagation distance of the excited wave was set to one meter based on experimental analysis. The sensor locations were assumed to be continuous variables. For clarity, a sketch illustrating the model constraints and terminology is presented in Figure 2.

The resulting problem is a non-convex problem with binary variables; therefore it is impossible to check whether the solution is a local or a global optimum. Therefore the quality of the generated solution will be dependent on the preliminary solution fed to the genetic algorithm. The initial sensor locations will be uniformly distributed on the surface.

Parameter notations

K : Set of control points
(x_k, y_k) : Coordinates of control point k
N : Number of PZT wafers to be placed
n : Coverage level
d_{min} : Minimum distance between each two PZTs
$d_{effective}$: Maximum spacing between the actuator-sensor pair
α_{min} : Minimum angle between two sensing paths
z : Path coverage
X : Set of points lying inside the geometry of the plate
R : Radius of the pipe

Decision variables

The definitions and equations of the current and the following sections are valid ∀:

$$k \in K; \quad i, j, i_1, j_1, i_2, j_2 \in N; \quad i < j; \quad i_1 < j_1; \quad i_2 < j_2.$$

(x_i, y_i) : coordinates of PZT wafer i
$C_k = \begin{cases} 1 \text{ if control point k is covered} \\ 0 \text{ otherwise} \end{cases}$
$C_{ijk} = \begin{cases} 1 \text{ if control point k is covered by PZT wafer line } (i,j) \\ 0 \text{ otherwise} \end{cases}$
d_{ij} = Direct distance between PZT wafer i and PZT wafer j
d'_{ij} = Indirect distance between PZT wafer i and PZT wafer j
d_{ijk} = Distance between PZT wafer line (i,j) and control point k
d_{ik} = Distance between PZT wafer i and control point k

The model is presented next

$$max \sum_{k \in K} C_k \tag{1}$$

Subject to:

$$d_{ij}^2 = \left(x_i - x_j\right)^2 + \left(y_i - y_j\right)^2 \tag{2}$$

$$d_{ij}'^2 = \left(2\pi \mathrm{R} - |x_i - x_j|\right)^2 + \left(y_i - y_j\right)^2 \tag{3}$$

$$d_{ik}^2 = (x_i - x_k)^2 + (y_i - y_k)^2 \tag{4}$$

$$d_{ijk} = \frac{|(y_j - y_i) \times x_k - (x_j - x_i) \times yk + x_j \times y_i - y_j \times x_i|}{\sqrt{(y_j - y_i)^2 + (x_j - x_i)^2}} \tag{5}$$

$$C_{ijk} = 0 \ \ if \ a_{ijk} + b_{ijk} < 1 \tag{6}$$

$$a_{ijk} = 0 \text{ if } d_{ijk} > z \tag{7}$$

$$a_{ijk} = 0 \text{ if } d_{ij} > d_{effective} \tag{8}$$

$$b_{ijk} = 0 \text{ if } d'_{ij} > z \quad (9)$$

$$b_{ijk} = 0 \text{ if } d'_{ij} > d_{effective} \quad (10)$$

$$C_k = 0 \; if \; \sum_{i \in N} \sum_{j \in N} C_{ijk} < n \quad (11)$$

$$C_{i_1 j_1 k} + C_{i_2 j_2 k} \leq 1 \; if \left| \frac{(x_{j_1} - x_{i_1}) \times (x_{j_2} - x_{i_2}) + (y_{j_1} - y_{i_1}) \times (y_{j_2} - y_{i_2})}{\sqrt{\left((x_{j_1} - x_{i_1})^2 + (y_{j_1} - y_{i_1})^2\right) \times \left((x_{j_2} - x_{i_2})^2 + (y_{j_2} - y_{i_2})^2\right)}} \right| > \cos \alpha_{min} \quad (12)$$

$$\min(d_{ij}, d'_{ij}) \geq d_{min} \quad (13)$$

$$(x_i, y_i) \in X \quad (14)$$

The major extension in this model is that the wave allowed to propagate in every direction (to allow for the continuous profile) and therefore any sensing element will receive two different signal corresponding to the short (direct) and long distance (indirect) between the actuator and the sensing element, as indicated in Figure 2. The direct and indirect distances between an actuator-sensor pair are calculated in equations (2) and (3) respectively.

Equations (4) and (5) calculate the distance between a PZT wafer and a control point k and the distance between the sensing path (i, j) and the control point k respectively. In equations (6-10), for a specific control point k to be covered by a path, the direct or indirect distances have to be less than z and $d_{effective}$. Equation (11) describes the required coverage level for all control points. Equation (12) summarizes the minimum angle constraint (α_{min}) which is the angle between each pair of paths. Equation (13) makes sure that the PZT wafers are separated by a distance $\geq d_{min}$. Equation (14) defines the plates geometry.

GA was used to solve the proposed models. A typical GA requires a genetic representation of the solution domain, and a fitness function to evaluate it. Each candidate solution is a chromosome of the number of genes equal to double the number of used PZTs; where each gene is an x or y coordinate value of a PZT element. Besides, the fitness function, to be maximized, is defined as the percentage of covered control points. Once these two elements (the genetic representation and the fitness function) are defined, a GA proceeds to initialize a population of solutions and then improve it through repetitive application of the mutation, crossover, inversion and selection operators. A population size of 200 was used in each generation to reduce the chance of getting a local optimum. “Rank” scaling function was used to give a scaled fitness value for every single individual in the population. The scaled fitness value of an individual is what defines its probability to be selected as a parent, using the “Stochastic uniform” selection function. The selected parents are used to form a second-generation population of solutions, through a combination of genetic operators including crossover and mutation. Five percent of the population, with the best fitness values, are chosen to pass to the next generation without undergoing crossover and mutation operations (the elite count is 5% of the population size).

The algorithm terminates when a maximum number of generations has been produced, a satisfactory fitness level has been reached for the population, or the highest-ranking solution's fitness has reached a plateau such that successive iterations no longer produce better results.

4 RESULTS AND DISCUSSION

The performance of the developed model was validated on a circular pipe. The main objective of the presented case is to demonstrate the robustness of the method in PZT wafer placement. The parameter n is a user defined attribute that can be controlled to achieve any level of coverage. Level 3 ($n = 3$) optimization was chosen, in this case, for demonstration on curved surfaces. During the optimization process, the selected number of sensors is the minimum N giving a coverage of at least 95%.

Sensor network optimization is performed on the surface of a 203.2 mm diameter and 1.2 meter long pipe. In the preliminary solution, the PZT wafers were distributed on the boundaries of upper and lower cross sections and on two axial lines on the surface of the pipe that are symmetric with respect to the z-axis of the pipe. The preliminary sensor network achieved 72% coverage. For the same number of sensors, 98% coverage was achieved in the optimized network. Both preliminary and optimized sensor networks are presented in Figure 3.

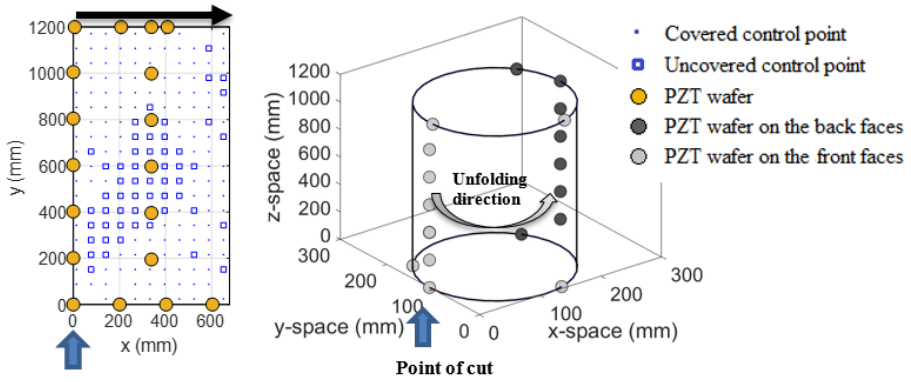

(a)

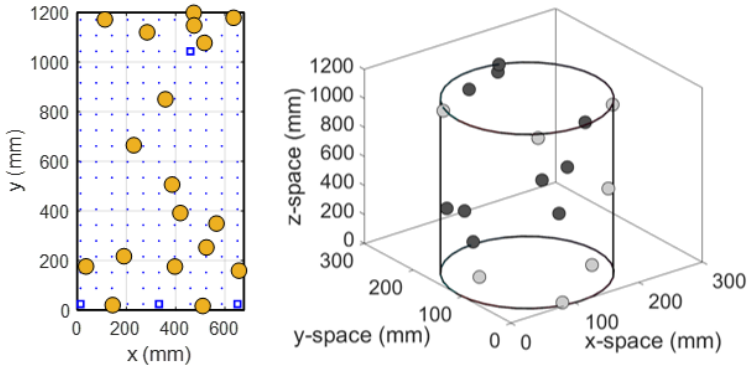

(b)

Figure 3. Sensor network optimization on the curved surface of the pipe (a) preliminary solution (72% coverage) and (b) optimized solution (98% coverage).

Figure 4 (a) shows the variation in coverage percentage with the number of sensors. It was shown that once a decent coverage is achieved (about 95%), any additional sensors may not contribute in a significant improvement in the coverage. Further, to check the repeatability of the results, based on the proposed optimization process, a fixed set of N (number of PZT wafers), known to give an optimized coverage percentage above 80%, was chosen. The optimized sensor network of each value of N (from the chosen set) was computed 10 times, separately. Figure 4 (b) shows the mean coverage percentage with error bars showing the variation among the 10 trials. A high stability in the percentage coverage was noticed, with a maximum standard deviation of 2.4%.

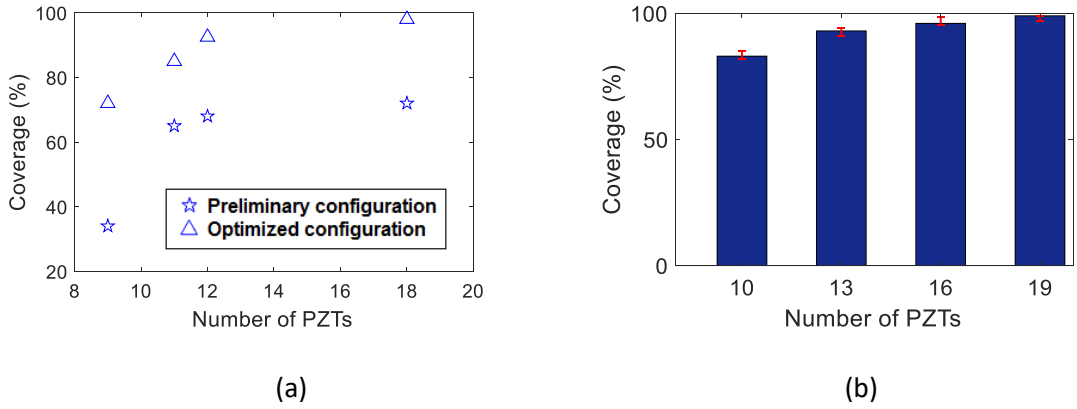

Figure 4. (a) The variation of the coverage versus the number of sensors and (b) mean coverage percentage of the 10 trials for different numbers of sensors.

Sensitivity analysis was performed to determine the importance of each sensor. For each sensor, the drop in coverage level is measured when this specific sensor is removed while maintaining the positions of all the other sensors, and then calculating the resulting coverage coverage. The process is repeated for all the sensors. The most important sensor is then identified as the sensor that caused the maximum drop in coverage. The coverage results are presented in Figure 5 (a). Because of the relatively large number of sensors used in the network, the drop of coverage is generally low.

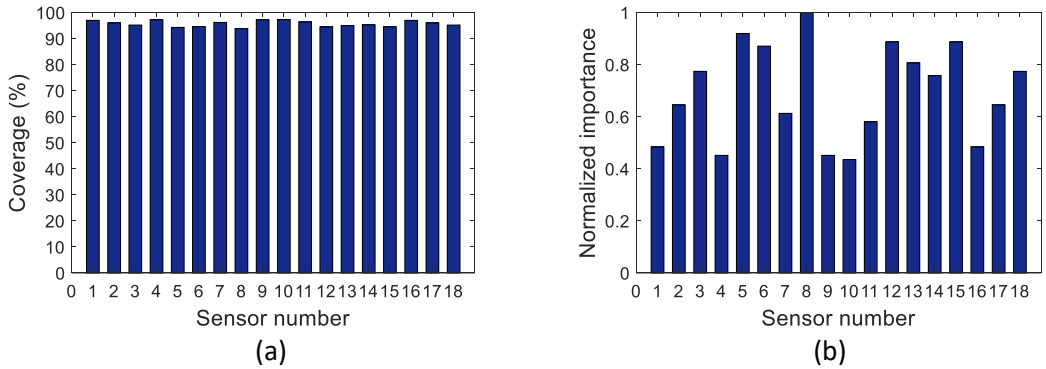

Figure 5. (a) Coverage after removing each sensor, (b) the normalized importance of the sensors.

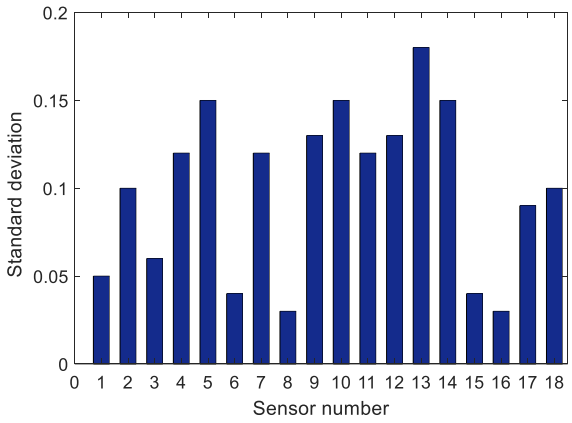

Figure 6. Standard deviation of the coverage when moving each sensor.

To verify the robustness of the results, a location sensitivity study is performed where the position of one sensor is varied by a random distance and direction (between -0.2 cm and 0.5 cm in the x-direction and between -0.5 cm and 0.5 cm in the y-direction) while keeping the other PZTs in their positions. This process is repeated for twenty times and the coverage was calculated every time the sensor is moved. Later, the mean and standard deviation of the coverages obtained were calculated. This procedure is repeated for all the sensors. Figure 6 shows the plot of the STD for each sensor. Indeed, all the standard deviations are very low. Thus, an error of 1 cm while installing sensors will have a minor effect on the coverage of the sensor network. This is expected in our cases where the coverage of the path is 0.03 m on either side.

5 CONCLUDING REMARKS

A novel approach for PZT-wafer-network placement on tubular structures, based on genetic algorithm, has been presented in this paper. The tubular structure is modelled as a plate with the appropriate boundary conditions imposed. The proposed objective function was to maximize the coverage of the monitored area, represented by a set of control points, while using the least possible number of sensors. Simulation results on a pipe section of 203.3 mm diameter and 1.2 meter in length showed a major improvement in the coverage level between the preliminary and optimized solutions. A coverage of 98% was achieved, based on the minimized number of sensors. Future, a sensitivity analysis was performed to determine the importance of each sensor within the network, in addition to the evaluation of the reduction in coverage due to slight misplacement of the PZT wafers. Future work will include experimental validations.

6 REFERENCES

Cawley, P. (2007). Practical guided wave inspection and applications to structural health monitoring. Proceedings of the 5th Australasian Congress on Applied Mechanics, Engineers Australia.

Davis, P. M., M. Spence and J.-F. Larivé (2016). Performance of European cross-country oil pipelines - Statistical summary of reported spillages in 2014 and since 1971 CONCAWE**:** 63.

Demma, A., P. Cawley, M. Lowe, A. Roosenbrand and B. Pavlakovic (2004). "The reflection of guided waves from notches in pipes: a guide for interpreting corrosion measurements." Ndt & E International **37**(3): 167-180.

Gazis, D. C. (1959). "Three-dimensional investigation of the propagation of waves in hollow circular cylinders. I. Analytical foundation." The journal of the Acoustical Society of America **31**(5): 568-573.

Guan, R., Y. Lu, W. Duan and X. Wang (2017). "Guided waves for damage identification in pipeline structures: A review." Structural Control and Health Monitoring **24**(11): e2007.

Huang, C.-F. and Y.-C. Tseng (2005). "The Coverage Problem in a Wireless Sensor Network." Mobile Networks and Applications **10**(4): 519-528.

Ismail, Z. M., M. A. H. Fakih, S. A. Mustapha and H. Tarhini (2018). The application of Genetic Algorithm for sensor placement of PZT wafers towards the application in structural health monitoring 12th European Conference on Non-Destructive Testing (ECNDT 2018). Gothenburg 2018, NDT.net.

Mustapha, S., L. Ye, D. Wang and Y. Lu (2011). "Assessment of debonding in sandwich CF/EP composite beams using A0 Lamb wave at low frequency." Composite Structures **93**(2): 483-491.

Seco, F. and A. R. Jiménez (2012). Modelling the generation and propagation of ultrasonic signals in cylindrical waveguides. Ultrasonic waves, InTech.

Silk, M. and K. Bainton (1979). "The propagation in metal tubing of ultrasonic wave modes equivalent to Lamb waves." Ultrasonics **17**(1): 11-19.

Tarhini, H., R. Itani, M. A. Fakih and S. Mustapha (2018). "Optimization of piezoelectric wafer placement for structural health-monitoring applications." Journal of Intelligent Material Systems and Structures **29**(19): 3758-3773.

Verma, B., T. K. Mishra, K. Balasubramaniam and P. Rajagopal (2014). "Interaction of low-frequency axisymmetric ultrasonic guided waves with bends in pipes of arbitrary bend angle and general bend radius." Ultrasonics **54**(3): 801-808.

Wang, X., W. T. Peter, C. K. Mechefske and M. Hua (2010). "Experimental investigation of reflection in guided wave-based inspection for the characterization of pipeline defects." NDT & e International **43**(4): 365-374.